



Seismic Performance of Gravity Retaining Walls Considering the Passive Soil at the Front Side

Orang Farzaneh¹ · Faradjollah Askari² · Peiman Sharifi³

Received: 2 May 2020 / Accepted: 22 October 2020 / Published online: 6 January 2021
© Indian Geotechnical Society 2021

Abstract There are many reasons to make behavior and performance of retaining walls during earthquakes difficult to evaluate, for example complex response of soil under dynamic loads, insufficiency of pseudo-static analyses, and the necessity for dynamic analyses. In recent years, progressive attention to the concept of performance-based design alleviated the situation and seismic displacement of retaining walls has got a critical role in the designing process of these structures. Furthermore, to economize the process of seismic design and reduce uncertainties coupled with pseudo-static methods, establishing a relationship between these methods and performance-based approaches provides a valuable tool for designers of geotechnical structures. In the present paper, by focusing on gravity walls and establishing applicable curves, relationships between the pseudo-static factor of safety, seismic coefficient, and seismic displacement have been investigated. In order to achieve this goal, the upper bound of limit analysis and integral of Newmark have been used. The height of the soil in the front of wall has been introduced as a design parameter. Fourteen selected Iran's earthquake records have been implemented in the process of analyses. The proposed curves can be used to determine the required embedment of a wall in the front soil and also for estimating the corresponding seismic displacement for specific

values of the seismic coefficient and factor of safety. Using the charts presented in this paper, it can be inferred that for a particular factor of safety (FS), greater values of seismic coefficient (k_h) provide smaller seismic displacements, and also, in greater values of k_h , the difference between values of seismic displacement of various FS will get close. Furthermore, for a certain k_h , increasing FS generates decreasing seismic displacements.

Keywords Gravity retaining wall · Seismic displacement · Performance · Factor of safety · Seismic coefficients

List of Symbols

FS	Pseudo-static factor of safety
k	Seismic acceleration coefficient
k_h	Horizontal seismic acceleration coefficient
k_v	Vertical seismic acceleration coefficient
k_y	Yield acceleration coefficient
a_h	Horizontal seismic acceleration
a_v	Vertical seismic acceleration
g	Gravity acceleration
φ_1	Internal friction angle of backfill
φ_2	Internal friction angle of soil at the front of wall
γ_1	Unit weight of backfill
γ_2	Unit weight of soil at the front of wall
γ_3	Unit weight of wall
θ	Backfill upper-hand angle with horizon
H_1	Height of wall and backfill
H_2	Height of soil mass at the front of wall
λ_1	Wall angle with backfill
λ_2	Wall angle with the soil at the front of wall
δ_1	Interface friction angles of the wall with backfill

✉ Peiman Sharifi
P.sharifi@ut.ac.ir

¹ Faculty of Engineering, University of Tehran, Tehran, Iran

² Geotechnical Engineering Research Center, International Institute of Earthquake Engineering and Seismology (IIEES), Tehran, Iran

³ Department of Civil Engineering, University of Tehran, Tehran, Iran

δ_2	Interface friction angles of the front soil	Ψ_1	Dilation angle of back wedge
δ_3	Interface friction angles of the wall with soil at the base of wall	Ψ_2	Dilation angle of front wedge
V	Volume	Ψ_3	Dilation angle of wall
S	Surface	Ψ_{31}	Dilation angle between the front wedge and the wall
T_i	External work rate of surface load	Ψ_{23}	Dilation angle between the back wedge and the wall
v_i	Deformation velocity	C	A parameter represents geometrical and mechanical characteristics of the wedges
X_i	External work rate of distributed forces	f_h	Horizontal force due to horizontal seismic acceleration
v_i^k	Kinematically admissible velocity field	f_v	Vertical force due to vertical seismic acceleration
σ_{ij}	Associated stress field	K_{ae}	Dynamic active pressure coefficient
$\dot{\epsilon}_{ij}$	Strain rate	K_{pe}	Dynamic passive pressure coefficient
\dot{u}_1	Velocity of back wedge	P_{ae}	Force acting on active wedge
\dot{u}_2	Velocity of front wedge	P_{pe}	Force acting on passive wedge
\dot{u}_3	Velocity of wall	R_v	Resultant of vertical forces acting upon the wall
\dot{u}_{31}	Relative velocity between wall and back wedge		
\dot{u}_{23}	Relative velocity between wall and front wedge		
d	Dissipated energy in the whole soil-wall system		
\dot{E}_{w1}	External work rate due to weights of the back wedge		
\dot{E}_{w2}	External work rate due to weights of the front wedge		
\dot{E}_{w3}	External work rate due to weights of the wall		
\dot{E}_{I1}	External work rate of back wedge due to inertial forces derived from acting horizontal seismic acceleration		
\dot{E}_{I2}	External work rate of front wedge due to inertial forces derived from acting horizontal seismic acceleration		
\dot{E}_{I3}	External work rate of wall due to inertial forces derived from acting horizontal seismic acceleration		
W_1	Weight of back-soil wedge		
W_2	Weight of front-soil wedge		
W	A general parameter for weight of wedges		
W_w and W_3	Weight of wall		
Q_1	Coefficient applied to velocity vector \dot{u}_1 to be converted to \dot{u}_3		
Q_2	Coefficient applied to velocity vector \dot{u}_2 to be converted to \dot{u}_3		
α	Critical angle of back wedge		
β	Critical angle of front wedge		
\ddot{u}_1	Acceleration of back wedge		
\ddot{u}_2	Acceleration of front wedge		
\ddot{u}_3	Acceleration of wall		
\ddot{u}_{31}	Relative acceleration between the front wedge and the wall		
\ddot{u}_{23}	Relative acceleration between the back wedge and the wall		

Introduction

Throughout the world, it is witnessed that earthquakes cause serious damages to structures and people's lives. Geotechnical structures play an essential role in diminishing a great part of these damages. Since gravity retaining wall is greatly used in many countries for lateral support, understanding their performances and behavior during an earthquake is highly recommended. The seismic performance of gravity retaining walls is considerably affected by permanent displacement caused by ground shaking, and conventional methods of seismic design of the walls cannot address the performance of walls. However, the emergence of the performance-based design minimized the number of uncertainties integrated with the conventional design methods. In these methods, not only the stability of structures is guaranteed but also their performances are considered in the designing process. During the twentieth century, several methods have been developed on stability analysis of retaining structures under seismic loads, and just over the last twenty years, the concept of performance-based design earned a proper amount of attention.

Until around 1960s, using the pseudo-static factor of safety (FS) was the most frequent method in seismic stability analysis of slopes and retaining walls. This approach compares the shear stresses required to maintain equilibrium with the available shear strength of soil [1]. The design seismic shear forces could be calculated by the pseudo-static method in which the forces derived by earthquake excitation were idealized by a specific seismic

coefficient. This method is simple and, nevertheless, gives no noteworthy information about seismic displacements of retaining walls at the end of an earthquake, i.e., about their seismic performance.

In the 1960s, Newmark [2] developed the sliding block method, which, despite its simplicity, brought a useful criterion to assess the seismic performance of slopes. Newmark stated that when $FS = 1$, horizontal seismic acceleration of slopes is actually the yield acceleration of the system. Double-time integration of the difference between the yield acceleration and actual earthquake acceleration results in permanent seismic displacement, i.e., whenever the system acceleration exceeds the yield acceleration, the whole structure starts to move. Since then, many geotechnical authors tried to expand this method, e.g., extending to other geotechnical structures. By some simplifying assumptions, Richards and Elms [3] expanded Newmark's method for retaining walls. Several numerical analyses took place after that to address retaining walls seismic displacement under various situations, to name a few, Nadim [4]; Nadim and Whitman [5], Rafnsson [6], and Rafnsson and Prakash [7]. Whitman and Liao [8] quantified the errors of Richards and Elms method discovered by other authors (Zarrabi-Kashani [9]) and modified the permanent seismic displacement formula generated by Richards and Elms. In 2006, Stamatopoulos et al. [10] proposed a model in which geometry changes of the backfill are accounted for in seismic displacement analyses. By using a kinematic approach of limit analysis and upper bound theorem, Michalowski [11] studied the displacement of slopes during seismic excitations considering multi-block analysis approach and acceleration hodographs. By using the limit equilibrium method, Trandafir et al. [12] analyzed the performance of reinforced retaining walls under earthquake loads and compared the displacement at the crest of the wall and backfill. Based on the limit analysis of upper bound theorem, Li et al. [13] studied the displacement of gravity retaining walls due to sliding and also the effect of vertical component of the seismic acceleration on the yield acceleration coefficient (k_y). Furthermore, they tried to consider wall roughness effects on the failure of the backfill soil. In 2013, Chowdhury and Singh [14] proposed an analytical solution to address the shortcomings of using Mononobe–Okabe [22, 23] in seismic evaluation of gravity retaining walls. Han et al. [15] investigated the effect of excess pore pressure in the rotational displacement of gravity quay retaining walls during earthquakes.

As it is mentioned, using seismic stability analysis was mainly focused on implementing FS before Newmark; even in the current state of the art, using FS is not obsolete at all. In recent years, a progressive gap has shaped between performance-based and conventional methods;

however, some authors tried to establish a relationship between FS and displacement-based analysis. Such methodologies can help practitioners to have a better understanding of the performance of geotechnical structures, which was previously designed by traditional methods, and even decrease the amount of uncertainty involved in designing by these approaches, e.g., choosing k_h based on a rational methodology, not on judgment and expertise of designers. There are many pieces of researches centered on the relationship of seismic displacement of slopes and their pseudo-static FS; on the other hand, there are a relatively small number of papers in the technical literature. Bozbey and Gundogdu [16] undertook such studies to propose charts to link seismic displacements, k_h , and FS using strong motion records taken during earthquakes in Turkey. Nadi et al. [17] generated charts with the same functionality focusing on seismic records of Iran. Biondi et al. [18] studied the seismic displacement of gravity retaining walls due to sliding failure. They proposed a particular definition of FS, which is the ratio of limit acceleration coefficient to earthquake-induced peak ground acceleration (maximum horizontal acceleration) on a system of two-wedge gravity retaining wall. In this study, limit acceleration coefficient defined as the peak horizontal acceleration coefficient required to induce a permanent displacement equal to the limit values of displacement, which could be calculated based on recommendations and guidelines for various situations. Accordingly, the proper k_h based on allowable seismic displacement was provided.

Methodology

In order to calculate the seismic displacement of gravity walls, Newmark method is used in this paper. In this method, the yield acceleration (k_y) plays the main role in calculating the seismic displacement. Whenever applied excitation passes this threshold acceleration, the system begins to deform. In this paper, for calculating k_y , a formulation based on the upper bound theorem of limit analysis is proposed. This process is applied to various values of FS. The pseudo-static analysis of Mononobe–Okabe [19, 20] is considered as the method to calculate FSs against sliding failure. In the following, first, the characteristics of considered gravity retaining walls will be described, and then, formulations for calculating the seismic displacement of gravity retaining walls will be provided.

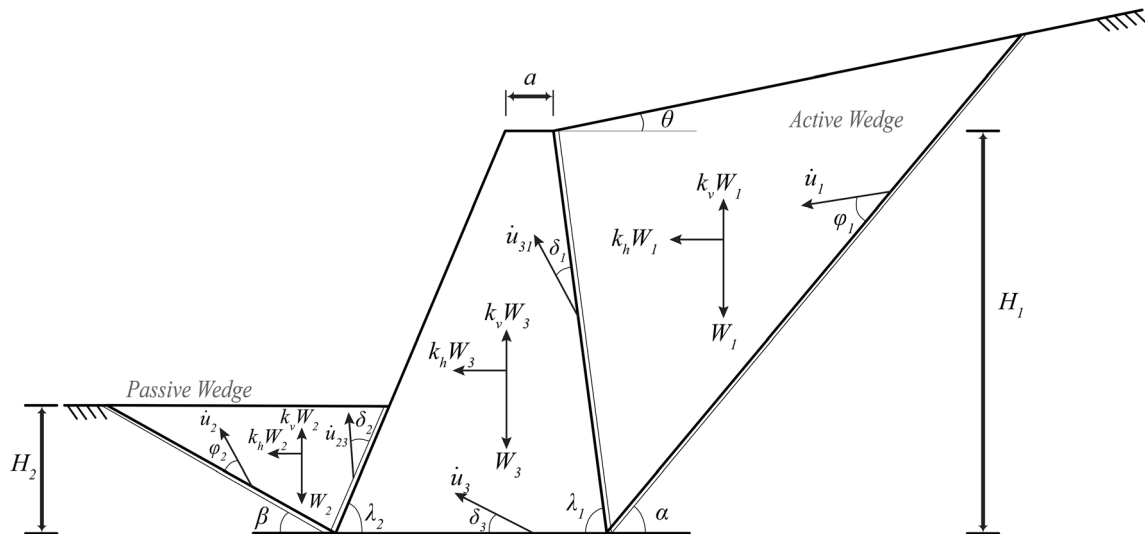


Fig. 1 Failure mechanisms of active and passive blocks

Characteristics of Considered Gravity Retaining Walls

Figure 1 shows a gravity retaining wall, which comprises three wedges. The soil mass with height H_1 that covers all the wall face, having the internal friction angle φ_1 and the unit weight γ_1 , is taken as the first wedge, which is inclined at an angle θ with the horizontal line. Correspondingly, soil mass at the front of wall with height H_2 , having an internal friction angle φ_2 and unit weight γ_2 , is considered as the second wedge, which has got a vertical fill. The wall itself is introduced as the third wedge with unit weight γ_3 , which is as high as the first wedge, and is inclined at angles λ_1 and λ_2 with the horizontal line next to the first and the second wedges, respectively. δ_1 , δ_2 , and δ_3 are interface friction angles of the wall with backfill, with the front soil, and with the soil at the base, respectively. It must be noted that all three wedges are considered dry.

Suggested Model for Permanent Seismic Displacements

In the current paper, a formulation based on the upper bound theorem of limit analysis is proposed to provide k_y , and based upon this value, Newmark’s sliding block is used as the method for calculation of seismic displacements of gravity retaining walls. In the following, assumptions are listed:

- All wedges are solid.
- The first and the second wedges follow the associated flow rule.
- The soil is dry and cohesionless.

Initiation of plastic deformation coincides with equality of stress state and yield condition of structure [11]. If the result of this condition forms a convex yield surface in the stress space, and the deformation is governed by the normality (or associative) flow rule, it can be concluded that in any kinematically admissible failure mechanism, the rate of internal work is not less than the rate of true external forces [21].

$$\int_V \sigma_{ij}^k \dot{\epsilon}_{ij}^k dV \geq \int_S T_i v_i dS + \int_V X_i v_i^k dV \tag{1}$$

The integral over entire volume V on the left side of Eq. (1) represents energy dissipated in entire mechanism, which is called the rate of internal work. Integral over entire boundary S on the right side introduces the external work rate of surface load T_i on S , which has got deformation velocity of v_i (kinematic boundary condition). The external work rate of distributed forces X_i per unit volume (such as weight, and inertial) in the kinematically admissible velocity field v_i^k is given by the latter integral in Eq. (1). Associated stress field σ_{ij} marked with superscript k is compatible with the selected mechanism [11]. $\dot{\epsilon}_{ij}$ is the strain rate compatible with real or virtual displacement rate v_i or v_i^k [22].

For the wall shown in Fig. 1, two parallel lines at each boundary of first and second wedges show failure surfaces, and the third wedge (the wall) slides along its base. As it is shown in Fig. 1, \dot{u}_1 , \dot{u}_2 and \dot{u}_3 are the velocities of the first, second and the third wedges; also, \dot{u}_{31} and \dot{u}_{23} represent the relative velocity between the wall and the first and the second wedges, respectively. Based on the associated flow rule, velocity vectors of wedges make specific angles with failure surfaces in kinematic boundary condition [23]. These angles between \dot{u}_1 and \dot{u}_2 and their corresponding

failure surfaces are φ_1 and φ_2 , and also their corresponding soil-wall failure surfaces are δ_1 and δ_2 , respectively. The angle between velocity vector of the wall and the base is δ_3 .

The velocity vectors of all three wedges form velocity hodographs. In Fig. 2, all possible shapes of velocity hodographs are shown.

Regarding Eq. 1, based on the upper bound theorem in the limit state, the rates of internal and external works in the soil wedges of Fig. 1 are as:

$$d \geq (1 - k_v) [\dot{E}_{w_1} + \dot{E}_{w_2} + \dot{E}_{w_3}] + k_h (\dot{E}_{I_1} + \dot{E}_{I_2} + \dot{E}_{I_3}) \quad (2)$$

where d represents the dissipated energy in the whole soil-wall system and k_v is the vertical seismic coefficient. \dot{E}_{w_1} , \dot{E}_{w_2} and \dot{E}_{w_3} , external work rates due to weights of the wedges, are:

$$\dot{E}_{w_1} = W_1 \dot{u}_1 \sin(\alpha - \phi_1) \quad (3a)$$

$$\dot{E}_{w_2} = -W_2 \dot{u}_2 \sin(\beta + \phi_2) \quad (3b)$$

$$\dot{E}_{w_3} = -W_3 \dot{u}_3 \sin \delta_3 \quad (3c)$$

Correspondingly, \dot{E}_{I_1} , \dot{E}_{I_2} and \dot{E}_{I_3} , external work rates due to inertial forces derived from acting horizontal seismic acceleration, are given by:

$$\dot{E}_{I_1} = W_1 \dot{u}_1 \cos(\alpha - \phi_1) \quad (4a)$$

$$\dot{E}_{I_2} = W_2 \dot{u}_2 \cos(\beta + \phi_2) \quad (4b)$$

$$\dot{E}_{I_3} = W_3 \dot{u}_3 \cos \delta_3 \quad (4c)$$

W_1 , W_2 , and W_3 are the weights of the back wedge, the front wedge, and the wall, respectively. α and β are the critical angles of back and front wedges, respectively. Assume the vertical seismic coefficient is a multiple of the horizontal seismic coefficient ($k_v = xk_h$) and also, assume as the failure occurs, the horizontal seismic coefficient equals yielding seismic coefficient ($k_y = k_h$). As long as the latter condition holds, Eq. (2) may be rewritten as

$$d = (1 - xk_y) [\dot{E}_{w_1} + \dot{E}_{w_2} + \dot{E}_{w_3}] + k_y (\dot{E}_{I_1} + \dot{E}_{I_2} + \dot{E}_{I_3}) \quad (5)$$

Q_1 and Q_2 are the coefficients applied to velocity vectors \dot{u}_1 and \dot{u}_2 to be converted to \dot{u}_3 . These coefficients, which are derived based on law of sines in each hodograph, are as follows:

$$\begin{cases} Q_1 = \frac{\sin(\lambda_1 - \delta_3 - \delta_1)}{\sin(\alpha + \lambda_1 - \phi_1 - \delta_1)} & (\delta_3 \geq \phi_1 - \alpha) \\ Q_1 = \frac{\sin(\pi - \lambda_1 + \delta_3 - \delta_1)}{\sin(\pi - \alpha - \lambda_1 + \phi_1 - \delta_1)} & (\delta_3 < \phi_1 - \alpha) \end{cases} \quad (6a)$$

$$\begin{cases} Q_2 = \frac{\sin(\lambda_2 + \delta_3 + \delta_2)}{\sin(\lambda_2 + \delta_2 + \phi_2 + \beta)} & (\phi_2 + \beta \geq \delta_3) \\ Q_2 = \frac{\sin(\lambda_2 + \delta_3 - \delta_2)}{\sin(\lambda_2 - \delta_2 + \phi_2 + \beta)} & (\phi_2 + \beta < \delta_3) \end{cases} \quad (6b)$$

Combining Eqs. (6) and (5) yields

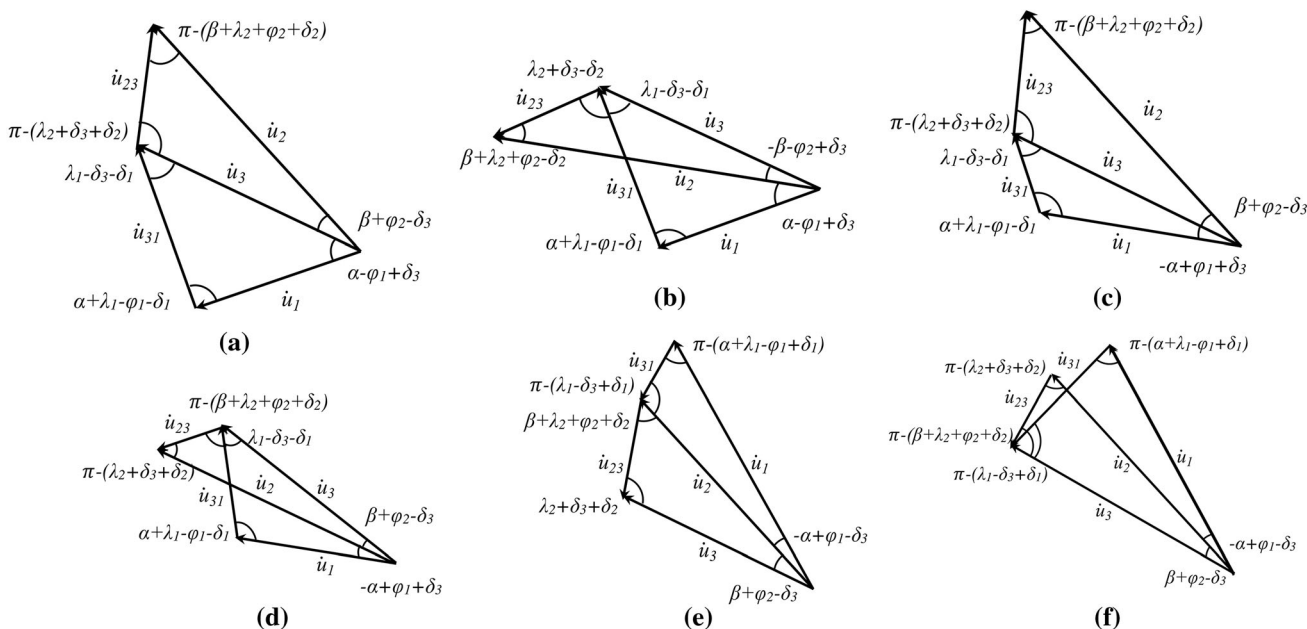


Fig. 2 Shapes of velocity hodographs

$$k_y = \frac{d - (Q_1 \dot{E}_{w_1} + Q_2 \dot{E}_{w_2} + \dot{E}_{w_3})}{(Q_1 \dot{E}_{l_1} + Q_2 \dot{E}_{l_2} + \dot{E}_{l_3}) - x(Q_1 \dot{E}_{w_1} + Q_2 \dot{E}_{w_2} + \dot{E}_{w_3})} \tag{7}$$

Since the soil is cohesionless, it can be concluded that in the above formula $d = 0$. As the upper bound theorem has been used, the desirable value for k_y would be derived by minimizing Eq. (7), with respect to α and β .

Once the seismic acceleration outweighs the yield acceleration ($k > k_y$), the sliding of the soil-wall system initiates. In other words, plastic deformations induce inertial forces due to seismic acceleration. The sliding at the first, the second, and the third wedges induces accelerations \ddot{u}_1, \ddot{u}_2 , and \ddot{u}_3 , respectively. As it is shown in Fig. 3, acceleration vectors make angles Ψ_1, Ψ_2 , and Ψ_3 with their corresponding failure surface, where Ψ_i is dilation angle. Relative acceleration and dilation angle between the first wedge and the wall equal to \ddot{u}_{31} and Ψ_{31} , respectively, and between the second wedge and the wall are \ddot{u}_{23} and Ψ_{23} , correspondingly. The current algorithm can consider $0 \leq \Psi_1 \leq \varphi_1$, $0 \leq \Psi_2 \leq \varphi_2$, $0 \leq \Psi_3 \leq \delta_3$, $0 \leq \Psi_{31} \leq \delta_3$, and $0 \leq \Psi_{23} \leq \delta_2$, but since it is assumed $\Psi_1 = \varphi_1$, $\Psi_2 = \varphi_2$, $\Psi_3 = \delta_3$, $\Psi_{31} = \delta_1$, and $\Psi_{23} = \delta_2$, acceleration hodographs are as the same as velocity hodographs shown in Fig. 2. It must be noted that work rates due to inertial forces are negative; this stems from the fact that wedge acceleration and acceleration vector are in opposite directions. The new energy balance equation is as follows.

$$d = -m_1 V_1 \ddot{u}_1 \cos(\phi_1 - \psi_1) - m_2 V_2 \ddot{u}_2 \cos(\phi_2 - \psi_2) - m_3 V_3 \ddot{u}_3 \cos(\delta_3 - \psi_3) + (1 - xk) \times [\dot{E}_{w_1} + \dot{E}_{w_2} + \dot{E}_{w_3}] + k(\dot{E}_{l_1} + \dot{E}_{l_2} + \dot{E}_{l_3}) \tag{8}$$

The following equation derived by substituting Eqs. (5) and (7) into Eq. (8).

$$\ddot{u}_3 = (k - k_y)g \frac{[m_1 Q_1 \cos(\alpha - \phi_1) + m_3 \cos(\delta_3) + m_2 Q_2 \cos(\phi_2 + \beta) - x(\dot{E}_{w_1} + \dot{E}_{w_2} + \dot{E}_{w_3})]}{[Q_1^2 m_1 \cos(\phi_1 - \psi_1) + Q_2^2 m_2 \cos(\phi_2 - \psi_2) + m_3 \cos(\phi_3 - \psi_3)]} = C(k - k_y)g \tag{9}$$

where k is the seismic acceleration coefficient and C is a parameter representing geometrical and mechanical characteristics of the wedges. Since real acceleration acts on wedges, double integration with respect to the time on both negative and positive acceleration directions and then choosing the larger value result in seismic displacement of gravity retaining wall:

$$u_3 = C \iint g(k - k_y) dt dt \tag{10}$$

A computer program was written in MATLAB [24] environment for the computation of permanent seismic displacement of a three-wedge gravity retaining walls system based on provided formula. The inputs are $H_1, H_2, a, \lambda_1, \lambda_2, \varphi_1, \varphi_2, \varphi_3, \delta_1, \delta_2, \delta_3, \gamma_1, \gamma_2, \gamma_3, \theta_1, \theta_2, k_h, k_v, FS$, and an earthquake record. The outputs are α, β, k_y, C , and the seismic displacement. The optimization algorithm used in this program pursues the procedure developed by Michalowski [20] and also Farzaneh and Askari [25]. This optimization uses the substitution of various combinations of $0 < \alpha, \beta < 90$ in Eq. (7) and estimates the minimum value of k_y .

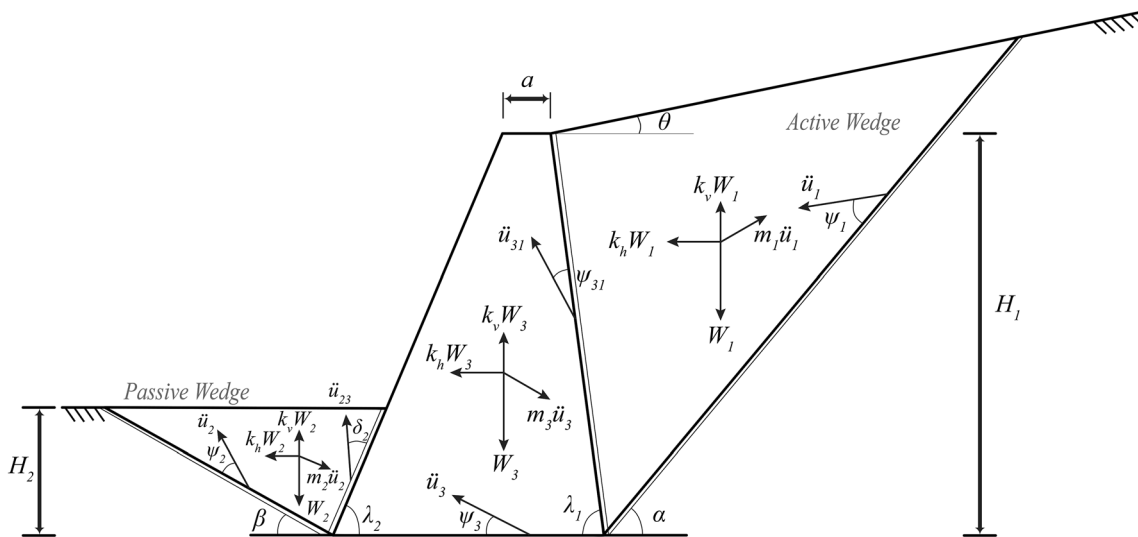


Fig. 3 Displacement mechanism of a gravity retaining wall

Pseudo-Static Factor of Safety

Okabe [20] and Mononobe and Matsuo [19] are architects of analyzing pseudo-static seismic forces acting on retaining structures known as Mononobe-Okabe method, which is a direct extension of Coulomb [26] approach [27].

As Mononobe–Okabe method is widely used in the practice, it is chosen as the method to calculate the pseudo-static factor of safety. As it is inferable by the name, the pseudo-static method, based on converting dynamic seismic forces to a static force, tries to evaluate the stability of geotechnical structures. For doing so, k_h and k_v are introduced as

$$k_h = \frac{a_h}{g} \tag{11}$$

$$k_v = \frac{a_v}{g} \tag{12}$$

where a_h , a_v , and g indicate horizontal seismic acceleration, vertical seismic acceleration, and gravity acceleration, respectively. It must be noted that coefficients of Eqs. (11) and (12) are dimensionless. Corresponding forces calculate as

$$f_h = k_h W \tag{13}$$

$$f_v = k_v W \tag{14}$$

where W is the weight of the (active or passive) soil blocks involved in the failure mechanism. The forces of Eqs. (4) and (5) add to static forces applying to gravity retaining walls.

P_{ae} and P_{pe} are forces acting on active and passive wedges, respectively, which are

$$P_{ae} = 0.5K_{ae}\gamma_1 H_1^2 (1 - k_v) \tag{15}$$

$$P_{pe} = 0.5K_{pe}\gamma_2 H_2^2 (1 - k_v) \tag{16}$$

where K_{ae} , dynamic active pressure coefficient, and K_{pe} , dynamic passive pressure coefficient, are Mononobe–Okabe’s coefficients which calculate as

$$K_{ae} = \frac{\cos^2(\phi_1 - 90 + \lambda_1 - \eta)}{\cos \psi \cos^2(90 - \lambda_1) \cos(\delta_1 + 90 - \lambda_1 + \eta) \left[1 + \sqrt{\frac{\sin(\delta_1 + \phi_1) \sin(\phi_1 - \theta_1 - \eta)}{\cos(\delta_1 + 90 - \lambda_1) \cos(\theta_1 - 90 - \lambda_1)}} \right]^2} \tag{17}$$

$$K_{pe} = \frac{\cos^2(\phi_2 - 90 + \lambda_2 - \eta)}{\cos \psi \cos^2(90 - \lambda_2) \cos(\delta_2 + 90 - \lambda_2 + \eta) \left[1 + \sqrt{\frac{\sin(\delta_2 + \phi_2) \sin(\phi_2 - \theta_2 - \eta)}{\cos(\delta_2 + 90 - \lambda_2) \cos(\theta_2 - 90 - \lambda_2)}} \right]^2} \tag{18}$$

β , λ_1 , λ_2 , θ_1 , and θ_2 are shown in Fig. 4 and $\eta = \arctan(k_h / (1 - k_v))$. It should be noted that the passive force values obtained by Mononobe-Okabe method are conservative [28]. In order to address the stability in the pseudo-static

method, FS against sliding, the most frequent failure in gravity retaining walls, is given by the ratio of resisting to driving forces, which for the wall shown in Fig. 4 calculates as

$$FS = \frac{R_v \tan(\delta_3) + P_{pe} \cos(\delta_2 + \lambda_2 - 90)}{P_{ae} \cos(90 + \delta_1 - \lambda_1) + k_h W_3} \tag{19}$$

In this formula, R_v , the resultant of vertical forces acting upon the wall, is:

$$R_v = (1 - k_v)W_3 + P_{ae} \sin(90 + \delta_1 - \lambda_1) - P_{pe} \sin(\delta_2 + \lambda_2 - 90) \tag{20}$$

Model Verification by Comparison with Literature

For a gravity retaining wall, like the one shown in Fig. 1, with $H_1 = 8$ m, $H_2 = 0$, $a = 0.3$ m, $\gamma_1 = 20$ kN/m³, $\lambda_1 = 90$, $\lambda_2 = 60.64$, $\delta_1 = 0$, $\theta_1 = 0$, $W_w = 556.8$ kN/m, where W_w is the weight of the wall, α and k_y are calculated and compared to the ones predicted by Li et al. [13]. These results, which are listed in Table 1, show a great match between these models.

Another gravity retaining wall with the following characteristics is used to compare the values of k_y and seismic displacement derived from proposed method over other methods: $H_1 = 4$ m, $H_2 = 0$, $a = 0.3$ m, $\gamma_1 = 21.6$ kN/m³, $\lambda_1 = 90$, $\lambda_2 = 62.3$, $\phi_1 = 33$, $\delta_1 = 22$, $\delta_3 = 23.3$, $\theta_1 = 0$, $W_w = 130.08$ kN/m. Values of seismic displacement have been calculated under Northridge 1994 earthquake, which its peak ground acceleration (PGA) and magnitude are 0.334 g and 6.69, respectively. Table 2 provides the results. It shows that the proposed model outcomes are close to the results provided by Mojallal and Ghanbari [29] and also Whitman and Liao [8].

For a gravity wall with $H_1 = 8$ m, $H_2 = 0$, $a = 1$ m, $\gamma_1 = 18$ kN/m³, $\lambda_1 = 90$, $\lambda_2 = 60.255$, $\phi_1 = 26$, $\delta_1 = 11$, $\delta_3 = 18$, $\theta_1 = 0$, $W_w = 634$ kN/m, Stamatopoulos et al’s [10] model predicts $\alpha = 54.2$ and $k_y = 0.016$; on the other hand, the proposed model estimates α and k_y equal to 54.10 and 0.0172, respectively. This comparison shows that the proposed model and Stamatopoulos et al’s [10] model are in very close agreement.

A Methodology Linking Seismic Displacement, Pseudo-Static Factor of Safety, and Horizontal Seismic Coefficient

In the current paper, by using records chosen by Mir-aboutalebi et al. [31] from seven earthquakes in transversal and longitudinal directions (fourteen records in total) recorded in Iran with various PGAs, values of seismic displacement of gravity retaining walls are calculated. Of course, a comprehensive conclusion for every location

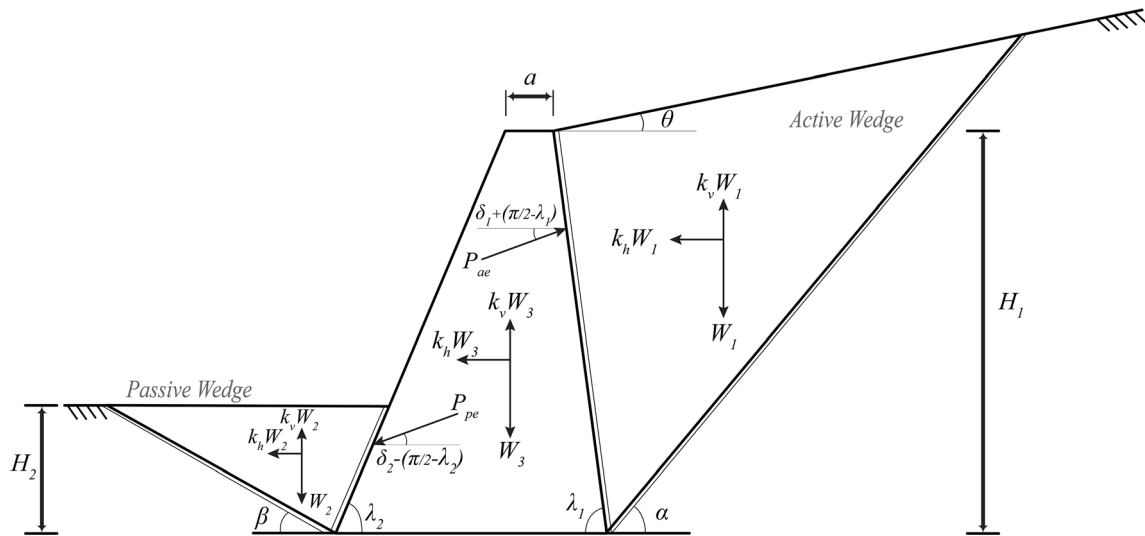


Fig. 4 Active and passive forces on a retaining wall

Table 1 Comparison of yield acceleration (k_y) and critical back-soil wedge failure angle (α)

φ_1	δ_3	k_y		α	
		Proposed method	Li et al. [13]	Proposed method	Li et al. [13]
25	25	0	0	57.50	57.9
30	30	0.111	0.11	54.67	55.2
35	35	0.224	0.22	52.03	55.0
40	40	0.340	0.34	49.49	49.5

Table 2 Comparison of yield acceleration (k_y) and seismic displacement

	Proposed method	Mojallal and Ghanbari [29]	Richards and Elms [3]	Whitman and Liao [8]	Wu [30]	
					Sliding	Combination of slide and rotation
k_y	0.098	0.097	0.155	0.1	–	–
Displacement (m)	0.153	0.167	0.095	0.118	0.062	0.166

cannot be provided by only this number of records, this said, these records have got acceptable extensiveness and acceptability. Table 3 provides information on the records.

In order to establish a relationship between seismic displacement, k_h and FS, geometric and mechanical characteristics of the wedges are introduced as follows. Internal friction angles of the backfill, front and the base soils are identical, and their values are 25, 30, 35, and 40 degrees. Also, $\delta_1 = \delta_2 = \delta_3 = 1/3\varphi, 2/3\varphi$. Moreover, for the wall shown in Fig. 1, $\theta = 0, 10, \lambda_1 = 70, 90, \lambda_2 = 80, k_v = 0$, and $a = 0.0375H_1$. Before introducing other parameters, it is worth-mentioning that after the development of the pioneer solution denoted as Mononobe–Okabe formulae, the effect of the vertical inertia force due to the vertical component of

the seismic acceleration has been always accounted in the evaluation of the seismic active and passive thrust. Furthermore, most of the pseudo-static approaches proposed in the literature for the seismic analyses of gravity retaining walls account for both k_h and k_v . Conversely, since the effect of the vertical component of the seismic acceleration is generally neglected in a displacement-based analysis carried out with a Newmark-type approach, in this framework, it is well known that its influence is almost negligible from a practical point of view. Accordingly, it is assumed that $k_v = 0$. It must be mentioned that the recommended seismic FS for gravity retaining walls in many references is 1.1. For more profound analyses, FS = 0.9, 1, 1.1, and 1.2 are considered too, and $H_2/H_1, C/\gamma H_2$ and γ_3/γ_1 are non-

Table 3 Characteristics of earthquake records of Iran [32]

Station	Location		Date D/M/Y	PGA cm/s/s	Magnitude		
	Longitude	Latitude			M_w	M_s	M_b
Deyhook	57.5	57.5	16/09/1978	410	–	7.4	6.4
Tabas	33.29	33.29	16/08/1978	897	–	7.4	6.4
Ab bar	56.92	56.92	20/06/1990	635	–	7.7	6.4
Meymand	33.58	33.58	20/06/1994	503	–	5.7	5.9
Zanjiran	48.97	48.97	20/06/1994	1006	–	5.7	5.9
Avaj	36.92	36.92	22/06/2002	498	6.5	6.4	6.2
Bam	52.75	52.75	26/12/2003	989	–	6.7	–

dimensional parameters derived from formulations. In order to analyze H_2/H_1 variation with k_h for considered values of FS, $C/\gamma H_{1,2} = 0$, $\gamma_3/\gamma_{1,2} = 1.22$, where $\gamma_2 = \gamma_1$ are obtained. The height of the soil in the front of the wall (H_2) can be calculated for a given characteristic of soil-wall system and a certain FS and k_h . Consequently, all geometric and mechanical parameters necessary for calculating k_y , α and β are given. With these parameters in hand, by using Newmark integration, seismic displacement of the gravity retaining wall for different records will be available too. The above-mentioned explanations can be depicted as a flowchart shown in Fig. 5.

and also the summation of logarithm of average and standard deviations of seismic displacement with k_h . Figure 7 shows similar curves for a wall with $\lambda_1 = 70$, $\lambda_2 = 80$, $a = 0.0375H_1$, $\varphi_1 = \varphi_2 = \varphi_3 = 35$, $\delta_1 = \delta_2 = \delta_3 = 2/3\varphi$, $\theta_1 = 0$. These curves help to link the seismic displacement of the gravity retaining wall to horizontal seismic coefficient and factor of safety. The dashed line in Figs. 6b, c and 7b, c shows the allowable seismic displacement equal to 2% of wall height [33].

Yet, for a wall with $\lambda_1 = 90$, $\lambda_2 = 80$, $a = 0.0375H_1$, $\varphi_1 = \varphi_2 = \varphi_3$, $\delta_1 = \delta_2 = \delta_3 = 1/3\varphi$, $2/3\varphi$, $\theta_1 = 0$, Fig. 8 shows k_y variation with H_2/H_1 for $\varphi = 25, 30, 35, 40$.

Numerical Results

Based on the described algorithm in the previous sections, for the wall shown in Fig. 1 with $H_1 = 8$ m, $\lambda_1 = 90$, $\lambda_2 = 80$, $a = 0.0375H_1$, $\varphi_1 = \varphi_2 = \varphi_3 = 40$, $\delta_1 = \delta_2 = \delta_3 = 2/3\varphi$, $\theta_1 = 10$ for various factors of safety, Fig. 6a shows H_2/H_1 variations with k_h ; Fig. 6b, c illustrates variations of logarithm of average seismic displacement

Discussion

To shed more light on the procedure of using these types of curves, examples are provided as follows: assume all of the wedges’ parameters are given as same as the ones contributed to represent Fig. 6. By using Fig. 6a and a certain k_h , one can generate H_2/H_1 values for various values of FS. Consider a situation in which the geotechnical designer

Fig. 5 The procedure of calculating the seismic displacement

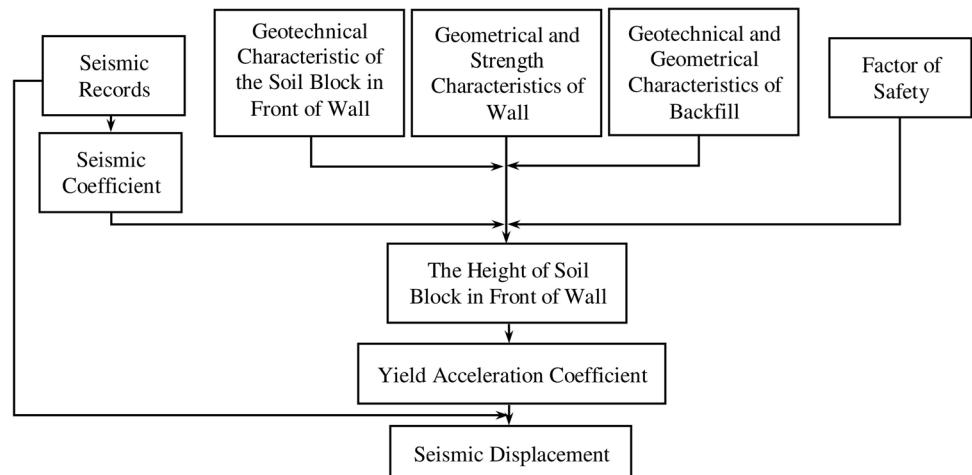
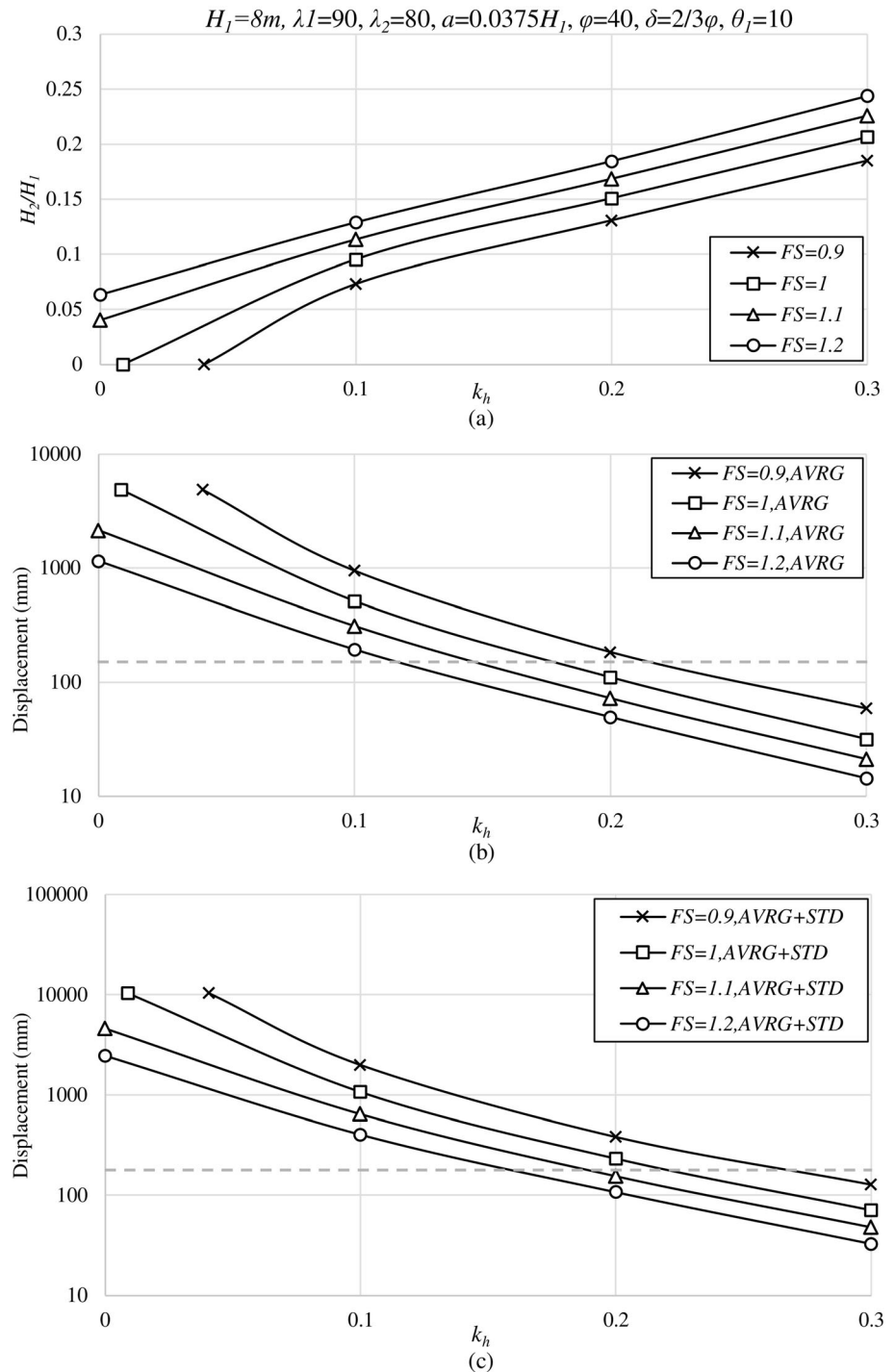


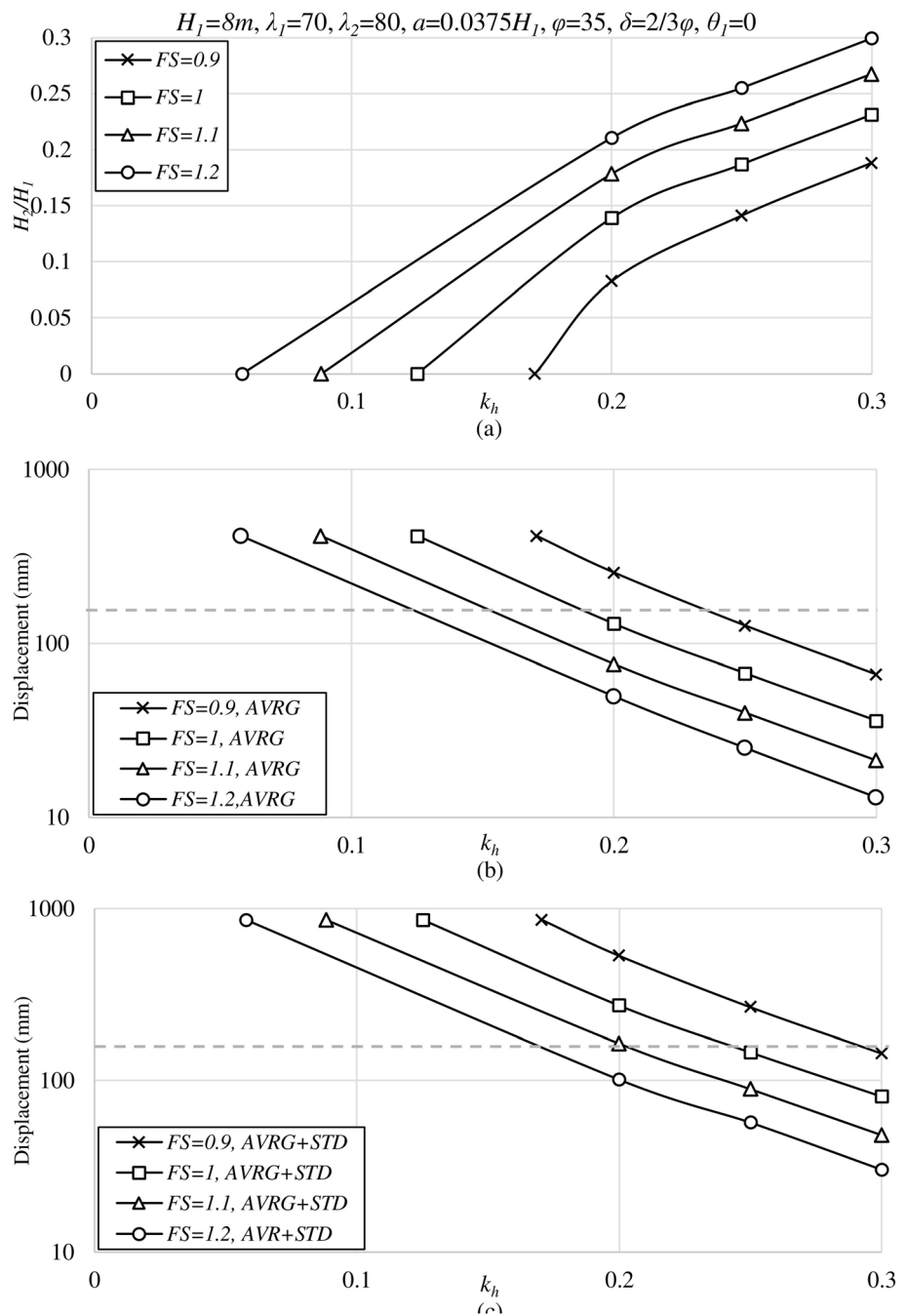
Fig. 6 k_h variation with **a** H_2/H_1 , **b** average seismic displacement and **c** summation of average and standard deviation of seismic displacement for different values of safety factors ($H_1 = 8$ m, $\lambda_1 = 90$, $\lambda_2 = 80$, $a = 0.0375H_1$, $\varphi = 40$, $\delta = 2/3\varphi$, $\theta_1 = 10$)



wants to determine the height of the soil in the front of a wall to have the optimum performance. This type of calculation may help the designer to have a deeper understanding of the height of fill in front of gravity retaining walls. The same procedure applies for determining FS based on a certain H_2/H_1 and k_h : For instance, consider FS = 1 and $k_h = 0.2$, H_2/H_1 equals 0.15 and vice versa, Fig. 6b, c brings seismic displacement into the circle, in

such a way that one can decide on a proper k_h to use in the pseudo-static analyses or on the other hand, estimating displacement during an earthquake (with k_h in hand) for a gravity wall. In other words, a designer can estimate the seismic displacement of a gravity wall just by having the factor of safety without undertaking time-consuming and expensive dynamic analysis. As an example, for the wall shown in Fig. 1, considering FS = 1.1, $H_2/H_1 = 0.185$ and

Fig. 7 k_h variation with **a** H_2/H_1 , **b** average seismic displacement and **c** summation of average and standard deviation of seismic displacement for different values of safety factors ($H_1 = 8$ m, $\lambda_1 = 70$, $\lambda_2 = 80$, $a = 0.0375H_1$, $\varphi = 35$, $\delta = 2/3\varphi$, $\theta_1 = 0$)



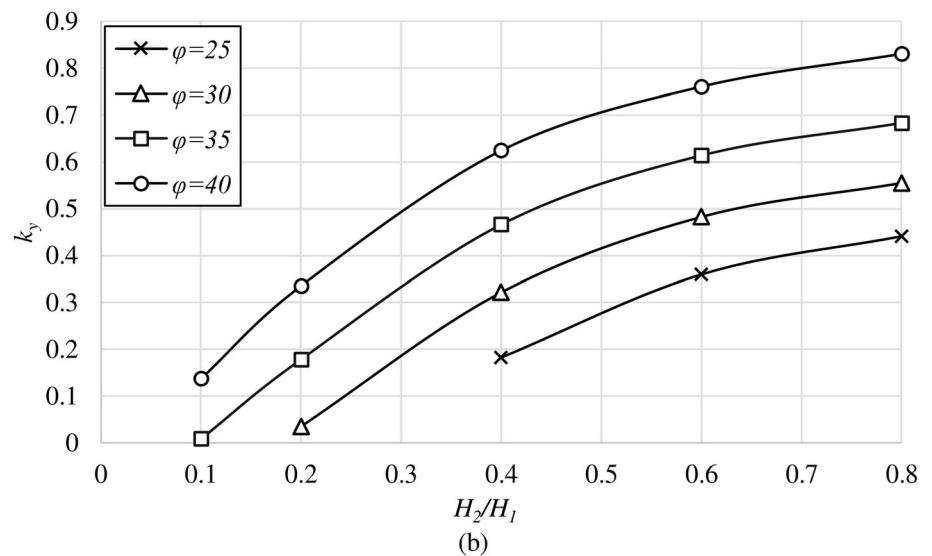
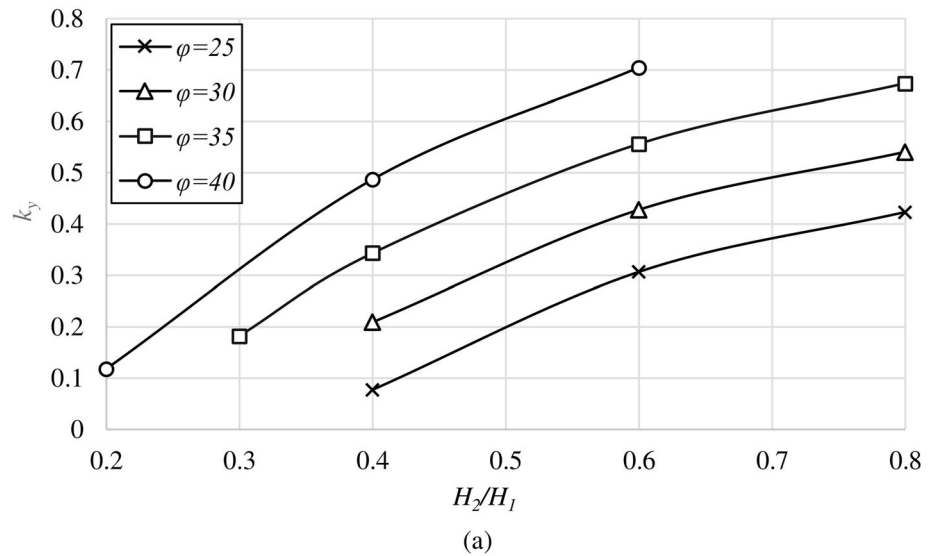
$k_h = 0.2$, by using Fig. 6a and c, the seismic displacement of the wall is equal to 72 mm.

The designer can also find the proper k_h based on allowable seismic displacement. There are many recommendations for allowable seismic displacement of gravity walls which can be found in various guidelines; for example, AASHTO LRFD Bridge Design Specifications suggest that horizontal wall displacement can be allowed as much as $250k_{h0}$ in millimeters. Similarly, Eurocode 8 [34] recommends $300k_{h0}$ in millimeters for allowable wall displacement. In both of these codes, the k_{h0} is equal to F_{PGA}

PGA. F_{PGA} is site factor at zero period on acceleration response spectrum which the values provided in tables for different site classes, and PGA is peak ground acceleration on rock.

Assuming $H_1 = 8$ m and using allowable displacement as 2% of wall height [33] in Fig. 6c, the desired k_h for FS = 1.1 approximately equals 0.14. Even the height of the wall at the front side of the wall can be determined based on allowable seismic displacement. In the process of choosing the permissible displacement, designers must keep in mind that different amount of displacement is

Fig. 8 k_y variation with H_2/H_1 for various φ values. **a** $\delta = \varphi/3$, **b** $\delta = 2\varphi/3$



required to fully mobilize the active and the passive soil thrust, which, according to the soil type for passive force, is 1.25–10 times larger than the corresponding displacement for active force [35]. This may help them to even choose more reasonable values of allowable seismic displacement.

Based on Fig. 6, for FS = 1.1, an increase in k_h values, from 0 to 0.3, results in $H_2/H_1 = 0.04$ –0.22. That is to say, in order to maintain the passive force against mobilized active force, H_2 must increase. In addition, for a special k_h , as it is inferable from Fig. 6a, larger H_2/H_1 is necessary to satisfy greater FS.

Figure 7 shows similar curves for a wall with $\lambda_1 = 70$, $\lambda_2 = 80$, $a = 0.0375H_1$, $\varphi_1 = \varphi_2 = \varphi_3 = 35$, $\delta_1 = \delta_2 = \delta_3 = 2/3\varphi$, $\theta_1 = 0$, which, at FS = 1.2, a rise in k_h from 0.057 to 0.3, declines the average values of seismic displacement from 416.3 to 13.04 mm. Generally stated, in a particular FS, using greater k_h values will provide smaller values for

seismic displacement. In greater values of k_h , the difference between values of seismic displacement of various FS will get close. Furthermore, for a certain k_h , increasing FS generates decreasing seismic displacements. It must be noted that the three charts shown in Figs. 6 and 7 must be considered simultaneously, and without taking into account the first chart (Figs. 6a, Fig. 7a), others are irrelevant. Figure 8 states that for a constant H_2/H_1 , higher values of φ leads to better seismic stability.

Summary and Conclusions

In this paper, a logical methodology was presented to establish a relationship between the pseudo-static factor of safety (FS), horizontal seismic coefficient (k_h), and seismic displacement of gravity retaining walls. In order to

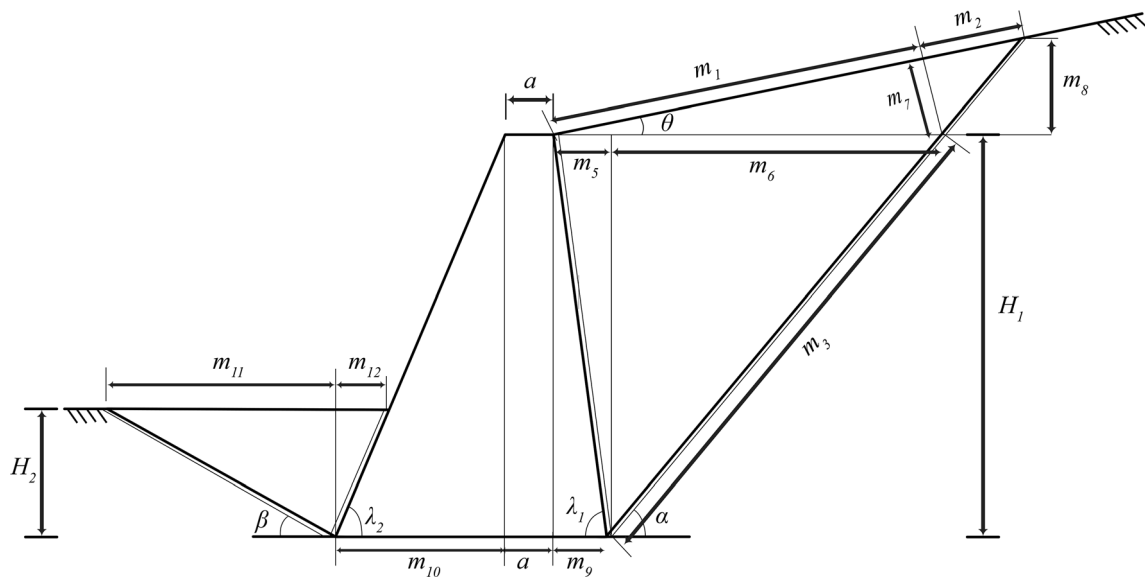


Fig. 9 Parameters used in wedges' weights calculation

determine seismic displacement of gravity retaining walls, a three-block failure mechanism was considered and the height of the soil in the front of the wall is taken into account. In order to determine the seismic displacement of the soil-wall system firstly, the yielding acceleration coefficient (k_y) was presented. To do so, a formulation based on the upper bound theorem of limit analysis was proposed. Then, using k_y along with the Newmark method the seismic displacement of gravity wall was calculated. In this study, some of strong motions data recorded in Iran are

used to carry out the Newmark displacement analysis, characterized by PGAs varying between 410 and 1006 cm^2/s^2 . Based on the provided algorithm, a series of charts presented which show the relationship between k_h , the ratio of the soil in front of the wall (H_2) to wall height (H_1) and average seismic displacement resulted from the aforementioned records. The various applications of these charts were described: Using these types of curves, one may generate H_2/H_1 values for different values of k_h and FS. Moreover, one can decide on a proper k_h to use in the

Fig. 10 Abbar **a** longitudinal and **b** transversal accelerograms

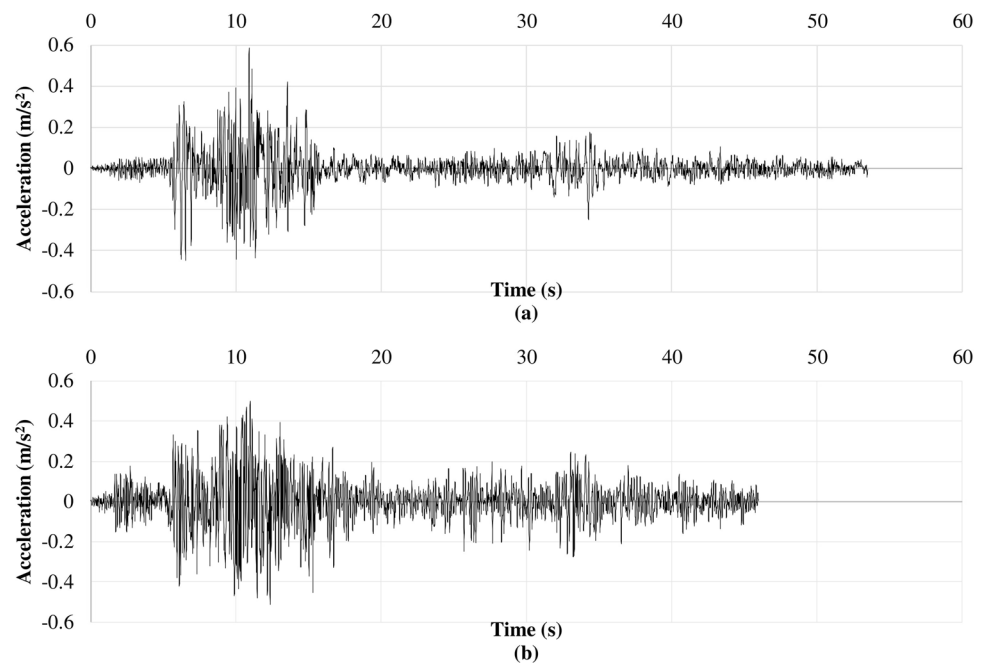


Fig. 11 Avaj **a** longitudinal and **b** transversal accelerograms

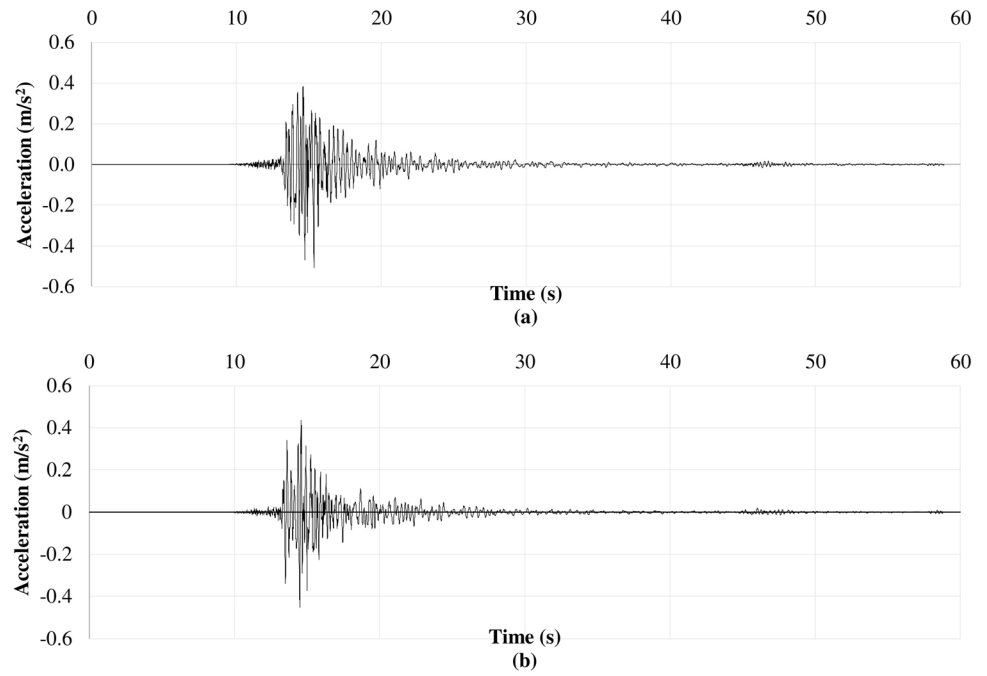


Fig. 12 Bam **a** longitudinal and **b** transversal accelerograms

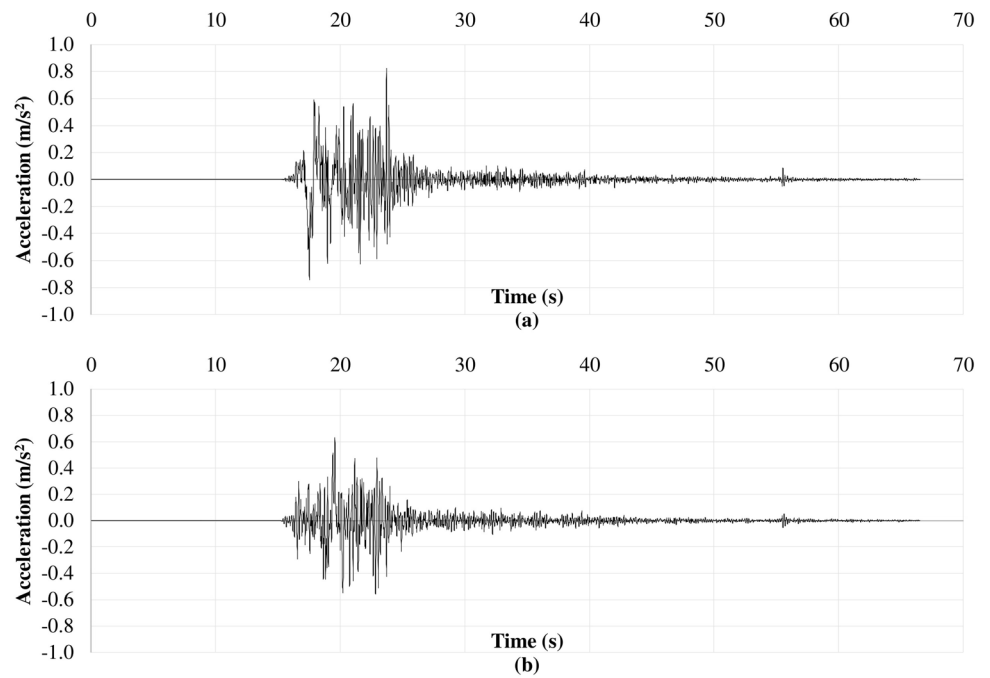


Fig. 13 Deihook **a** longitudinal and **b** transversal accelerograms

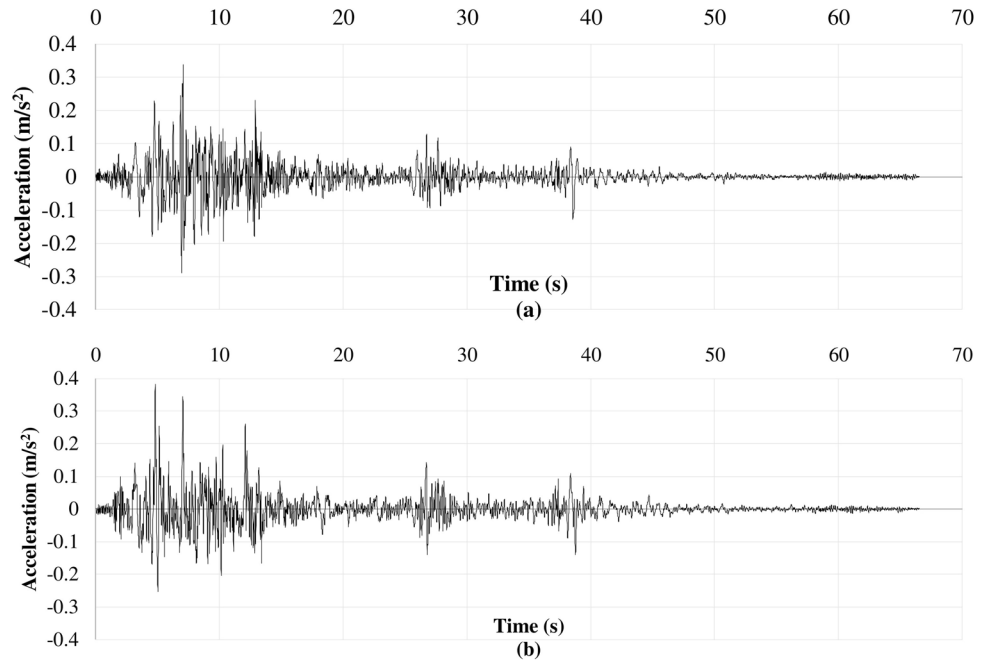


Fig. 14 Meymand **a** longitudinal and **b** transversal accelerograms

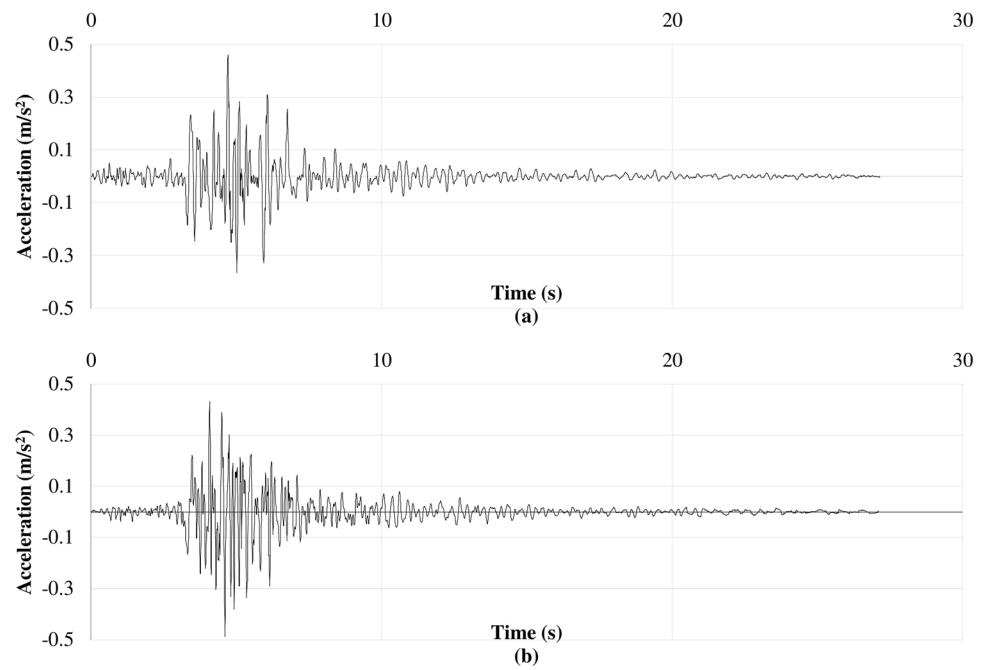


Fig. 15 Tabas **a** longitudinal and **b** transversal accelerograms

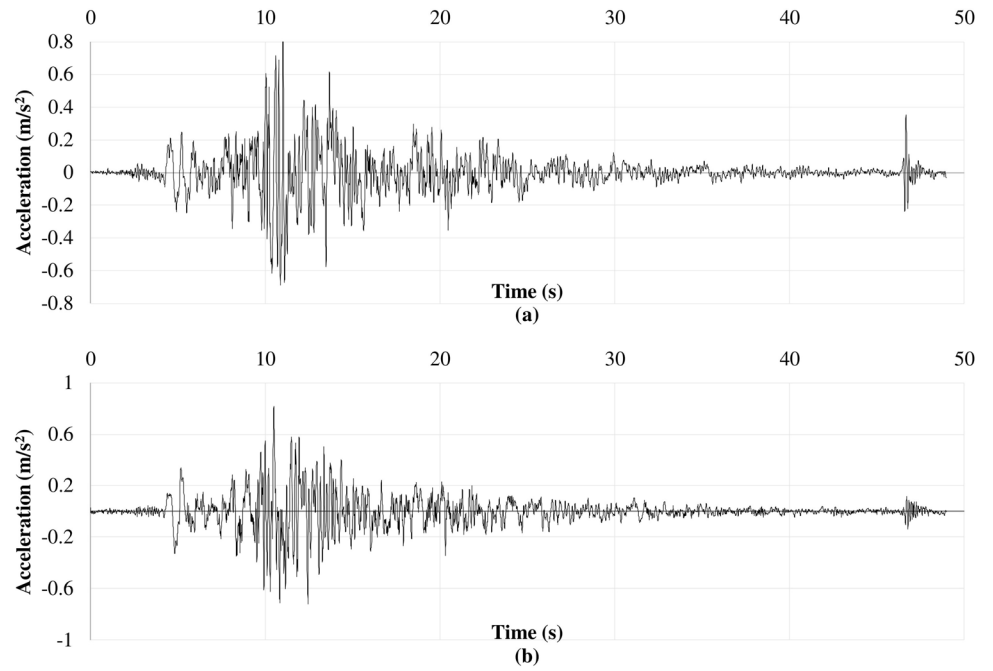
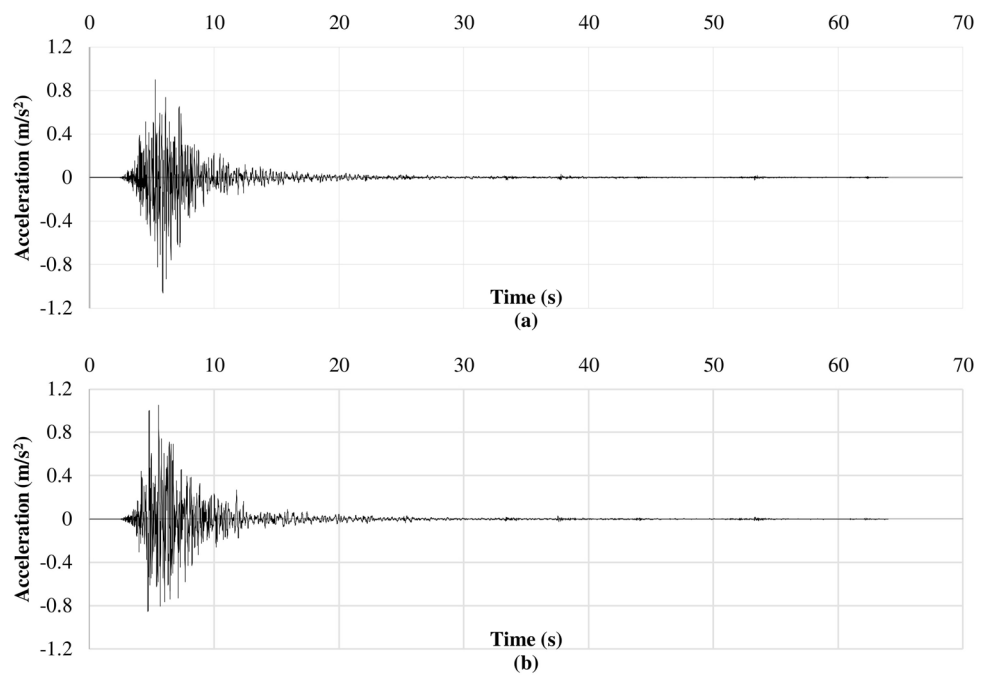


Fig. 16 Zanjiran **a** longitudinal and **b** transversal accelerograms



pseudo-static analyses or estimate displacement during an earthquake (with a particular k_h) for a gravity wall. The effect of various values of internal frictional angle of soil on yielding acceleration coefficient was also investigated.

Acknowledgements This paper is prepared based on results of MSc thesis of the third author in Tehran University (Faculty of Engineering) and in the framework of researches on seismic design of walls in continuation and development of the research project No. 403/6718 in International Institute of earthquake Engineering and Seismology (IIEES). The supports are acknowledged.

Appendix A

According to Fig. 9, wedge dimensions calculate as

$$m_5 = \frac{H_1}{\tan \lambda_1} \tag{21}$$

$$m_6 = \frac{H_1}{\tan \alpha} \tag{22}$$

$$m_1 = (m_5 + m_6) \cos \theta = H_1 \left(\frac{1}{\tan \lambda_1} + \frac{1}{\tan \alpha} \right) \cos \theta \tag{23}$$

$$m_7 = m_1 \tan \theta = H_1 \left(\frac{1}{\tan \lambda_1} + \frac{1}{\tan \alpha} \right) \sin \theta \tag{24}$$

$$m_2 = \frac{m_7}{\tan(\alpha - \theta)} = \frac{H_1 \sin \theta}{\tan(\alpha - \theta)} \left(\frac{1}{\tan \lambda_1} + \frac{1}{\tan \alpha} \right) \tag{25}$$

$$m_3 = \frac{H_1}{\sin \alpha} \tag{26}$$

$$m_8 = (m_1 + m_2) \sin \theta = H_1 \sin \theta \left(\frac{1}{\tan \lambda_1} + \frac{1}{\tan \alpha} \right) \tag{27}$$

$$m_4 = \frac{m_8}{\sin \alpha} = H_1 \left(\frac{\sin \theta}{\sin \alpha} \right) \left(\frac{1}{\tan \lambda_1} + \frac{1}{\tan \alpha} \right) \tag{28}$$

$$m_9 = m_5 \tag{29}$$

$$m_{10} = \frac{H_1}{\tan \lambda_2} \tag{30}$$

$$m_{11} = \frac{H_2}{\tan \beta} \tag{31}$$

$$m_{12} = \frac{H_2}{\tan \lambda_2} \tag{32}$$

Then, the weights of wedges are given as below.

$$W_1 = \gamma_1 (m_5 + m_6) \left(\frac{H_1}{2} + \frac{m_8}{2} \right) \tag{33}$$

$$W_2 = (m_{11} + m_{12}) \left(\frac{H_2 \gamma_2}{2} \right) \tag{34}$$

$$W_3 = (2a + m_9 + m_{10}) \left(\frac{\gamma_3 H_1}{2} \right) \tag{35}$$

Appendix B

The accelerograms of the earthquake’s records used in the paper are provided here. These records are all obtained from International Institute of Earthquake Engineering and Seismology (IIEES) [32] of Iran (Figs. 10, 11, 12, 13, 14, 15, 16).

References

- Kramer SL (2014) Performance-based design methodologies for geotechnical earthquake engineering. *Bull Earthq Eng* 12(3):1049–1070
- Newmark NM (1965) Effects of earthquakes on dams and embankments. *Geotechnique* 15(2):139–160
- Richards Jr R, Elms DG (1979) Seismic behavior of gravity retaining walls. *J Geotech Geoenviron Eng* 105(ASCE 14496)
- Nadim F (1982) A numerical model for evaluation of seismic behavior of gravity retaining walls. Massachusetts Institute of Technology, Cambridge
- Nadim F, Whitman RV (1983) Seismically induced movement of retaining walls. *J Geotech Eng* 109(7):915–931
- Rafnsson, E. A. (1993). Displacement-based design of rigid retaining walls subjected to dynamic loads considering soil nonlinearity
- Rafnsson EA, Prakashtnain S (1994) Displacement based aseismic design of retaining walls. In: International conference on soil mechanics and foundation engineering, pp 1029–1032
- Whitman RV, Liao S (1985) Seismic design of gravity retaining walls. Massachusetts Inst of Tech Cambridge Dept of Civil Engineering
- Zarrabi-Kashani K (1979) Sliding of gravity retaining wall during earthquakes considering vertical acceleration and changing inclination of failure surface (Doctoral dissertation, Massachusetts Institute of Technology)
- Stamatopoulos CA, Velgaki EG, Modaressi A, Lopez-Caballero F (2006) Seismic displacement of gravity walls by a two-body model. *Bull Earthq Eng* 4(3):295–318
- Michalowski RL (2007) Displacements of multiblock geotechnical structures subjected to seismic excitation. *J Geotech Geoenviron Eng* 133(11):1432–1439
- Trandafir AC, Kamai T, Sidle RC (2009) Earthquake-induced displacements of gravity retaining walls and anchor-reinforced slopes. *Soil Dyn Earthq Eng* 29(3):428–437
- Li X, Wu Y, He S (2010) Seismic stability analysis of gravity retaining walls. *Soil Dyn Earthq Eng* 30(10):875–878
- Chowdhury I, Singh JP (2014) Performance evaluation of gravity type retaining wall under earthquake load. *Indian Geotech J* 44(2):156–166
- Han S, Gong J, Zhang Y (2017) Seismic rotational displacements of gravity quay walls considering excess pore pressure in backfill soils. *J Earthq Eng* 21(6):985–1009
- Bozbey I, Gundogdu O (2011) A methodology to select seismic coefficients based on upper bound “Newmark” displacements using earthquake records from Turkey. *Soil Dyn Earthq Eng* 31(3):440–451

17. Nadi B, Askari F, Farzaneh O (2014) Seismic performance of slopes in pseudo-static designs with different safety factors. *Iran J Sci Technol Trans Civ Eng* 38(C2):465
18. Biondi G, Cascone E, Maugeri M (2014) Displacement versus pseudo-static evaluation of the seismic performance of sliding retaining walls. *Bull Earthq Eng* 12(3):1239–1267
19. Mononobe N, Matsuo H (1929) On the determination of earth pressure during earthquakes. In: *Proceedings of the world engineering congress, Tokyo*, vol 9, p 388
20. Okabe S (1924) General theory of earth pressure and seismic stability of retaining wall and dam. *J Jpn Soc Civ Eng* 10(6):1277–1323
21. Drucker DC, Prager W, Greenberg HJ (1952) Extended limit design theorems for continuous media. *Q Appl Math* 9(4):381–389
22. Chen WF (ed) (2013) *Limit analysis and soil plasticity*. Elsevier, Amsterdam
23. Green RA, Michalowski RL (2006) Shear band formation behind retaining structures subjected to seismic excitation. *Found Civ Environ Eng* 7:157–169
24. MATLAB (2010) Version 7.10.0 (R2010a). The MathWorks Inc, Natick
25. Farzaneh O, Askari F (2003) Three-dimensional analysis of nonhomogeneous slopes. *J Geotech Geoenviron Eng* 129(2):137–145
26. Coulomb CA (1776) An attempt to apply the rules of maxima and minima to several problems of stability related to architecture. *Mémoires de l'Académie Royale des Sciences* 7:343–382
27. Kramer S (1996) *Geotechnical earthquake engineering*. Prentice-Hall Inc, New York
28. AASHTO LRFD (1998) *Bridge design specifications*. American Association of State Highway and Transportation Officials, Washington, D.C.
29. Mojallal M, Ghanbari A (2012) Prediction of seismic displacements in gravity retaining walls based on limit analysis approach. *Struct Eng Mech* 42(2):247–267
30. Wu Y (1999) *Displacement-based analysis and design of rigid retaining walls during earthquakes*. Doctoral Dissertations. 1309. https://scholarsmine.mst.edu/doctoral_dissertations/1309
31. Miraboutalebi M, Askari F, Farzaneh O (2011) Effect of bedrock inclination on seismic slope stability according to Iran seismically data. *Int J Civ Eng* 9:247–254
32. International Institute of Earthquake Engineering and Seismology. Available at: <http://www.iiées.ac.ir/en/>
33. Wu Y, Prakash S (1996) On seismic displacements of rigid retaining walls. In: *Analysis and design of retaining structures against earthquakes*, pp 21–37
34. British Standards Institution (1996) *Eurocode 8: design provisions for earthquake resistance of structures*. British Standards Institution, London
35. Das, B. M. (2015). *Principles of foundation engineering*. Cengage learning

Publisher's Note Springer Nature remains neutral with regard to jurisdictional claims in published maps and institutional affiliations.